AIAA JOURNAL
Vol. 44, No. 7, July 2006

Validation Case Study: Prediction of Compressible Turbulent Mixing Layer Growth Rate

M. F. Barone,* W. L. Oberkampf,† and F. G. Blottner‡
Sandia National Laboratories, Albuquerque, New Mexico 87185

DOI: 10.2514/1.19919

A recently developed validation metric is applied to the example problem of growth-rate prediction for a turbulent, compressible mixing layer. Emphasis is placed on the validation exercise as a well-defined process, which must include quantification of numerical error, evaluation of the level of confidence in the experimental data, and estimation of model accuracy. Available data for compressible mixing layers are reexamined, resulting in a new recommended data set for the study of mixing layer growth rate. Numerical solutions to the Favre-averaged Navier–Stokes equations with various two-equation turbulence closures and compressibility models are obtained and verified through formal solution verification procedures. The validation metric results are presented for each of the models, including local error estimates for detailed evaluation of model performance and global metrics that facilitate model performance comparisons.

Nomenclature

C_b, C_s, C_ω	=	error function profile growth-rate constants
$\lvert\frac{\bar{CI}}{\bar{y}_e}\rvert_{\text{avg}}$	=	normalized confidence interval average width
$\lvert\frac{CI}{\bar{y}_e}\rvert_{\max}$	=	normalized confidence interval maximum width
E_b, E_s, E_ω	=	hyperbolic tangent profile growth-rate constants
$\lvert\frac{\bar{E}}{\bar{y}_e}\rvert_{\text{avg}}$	=	average relative error
$\lvert\frac{\bar{E}}{\bar{y}_e}\rvert_{\max}$	=	maximum relative error
M	=	Mach number
N_i	=	no. streamwise grid cells
N_j	=	no. cross-stream grid cells
p	=	spatial convergence rate
$S(\boldsymbol{\theta})$	=	error sum of squares
T	=	temperature
T_0	=	total temperature
u	=	streamwise velocity
x	=	streamwise coordinate
y	=	cross-stream coordinate
$\beta_0, \beta_1, \beta_2$	=	thickness fit parameters
$\Delta y_1, \Delta y_2$	=	grid spacing parameters
$\mathrm{d}\delta/\mathrm{d}x$	=	mixing layer growth rate
ε	=	estimated fractional error
$\hat{\boldsymbol{\theta}} = \hat{\theta}_1, \hat{\theta}_2, \hat{\theta}_3$	=	regression coefficients
μ	=	viscosity
μ_T	=	eddy viscosity
ρ	=	density
σ	=	spreading rate parameter
σ_0	=	spreading rate parameter constant

Subscripts

c	=	compressible
i	=	incompressible
1	=	fast stream
2	=	slow stream

Introduction

As computational fluid dynamics (CFD) and other numerical tools are used more routinely for design, analysis, and risk assessment, the question of how to validate such tools is paramount. Validation of physics models is often not carried out in a rigorous, or even systematic, fashion. This is partly due to the lack of *practical* and well-defined procedures for comparing predictive computational results with physical truth (reliable experiments).

Recently, a new validation metric has been proposed that allows practical quantitative evaluation of the accuracy of a deterministic computational model, relative to an experimental data set [1,2]. The key features of the validation metric are repeated here:

1) Assessment of numerical error is not explicitly treated by the validation metric. The numerical error must be shown to be negligible before application of the metric.

2) The metric is a quantitative measure of the accuracy of the model in predicting a specific system response quantity (SRQ). This measure is an aggregate one that includes all aspects of the physical model.

3) The metric includes an estimation of error associated with the experimental data, including measurement errors and postprocessing errors.

4) The metric depends on the number of experimental measurements used to validate the model.

5) The metric excludes any indication of the level of adequacy of the agreement with experiment.

The primary purpose of this paper is to present a detailed procedure for application of such a validation metric. The chosen example is the validation of compressibility corrections to two-equation turbulence models for prediction of the growth-rate reduction in a turbulent, planar, compressible mixing layer. This example is a common unit-level validation problem used to assess turbulence closures for the Favre-averaged Navier–Stokes equations. In this work we consider the performance of various two-equation turbulence models with well-known and presently available compressibility corrections.

Emphasis has been placed on the sequential steps in a careful validation process:

Received 6 September 2005; revision received 20 February 2006; accepted for publication 6 March 2006.

*Senior Member of Technical Staff, Aerosciences and Compressible Fluid Mechanics Department, P.O. Box 5800 MS 0825; mbarone@sandia.gov. AIAA Member.

†Distinguished Member of Technical Staff, Validation and Uncertainty Quantification Department, MS 0828. AIAA Fellow.

‡Consultant, Aerosciences and Compressible Fluid Mechanics Department, MS 0825. AIAA Fellow.

1) Consistent specification of the SRQ of interest that will be used to compare computation with experiment.

2) Careful postprocessing of the SRQ from both the experiment and the computation.

3) Numerical solution verification efforts.

4) Quantitative comparison of model performance via both local and global validation metrics.

Each of these steps is described in detail for the mixing layer validation problem.

In the process of assembling experimental data for this validation study, the authors carried out a detailed evaluation of the reported growth-rate results for the compressible mixing layer. A consistent means of postprocessing the reported experimental results was developed and is presented in detail in the next section. Typical ensembles of such data usually result in significant spread of the data, with resulting ambiguity in evaluation of physical modeling of compressible mixing layers. The data set presented below, although it has some deficiencies to be discussed later, will, it is hoped, serve as useful validation data for future studies. A secondary goal of this study is to highlight further needs in both the modeling and experimental communities in the area of compressible turbulent shear flows.

An introduction to the compressible shear layer problem is given in the next section, including the discussion of a consistent experimental data set with which to compare the models. Details of the computational models and verification of the numerical solutions are described in the following section. Finally, the validation metric results are presented and discussed.

Problem Description

Figure 1 shows the general flow configuration; a thin splitter plate separates two streams of gas (numbered 1 and 2, where $u_1 > u_2$) with distinct flow velocities and temperatures. The two streams mix downstream of the splitter plate trailing edge, forming the free shear layer within which momentum and energy are mixed and diffused. For high-Reynolds number flow, the boundary layers on both sides of the plate and the free shear layer are inevitably turbulent. In the absence of any applied pressure gradients or other external influences, the flowfield downstream of the trailing edge consists of a shear layer development region near the edge, followed by a similarity region. Within the development region the shear layer adjusts from its initial velocity and temperature profiles inherited from the plate boundary layers. Further downstream, the shear layer attains similarity profiles. The key characteristic of the similarity region is that the shear layer thickness $\delta(x)$ grows linearly with streamwise distance x.

Of particular interest in high-speed applications is the behavior of the shear layer as the effective Mach number of convecting turbulent eddies increases. A widely accepted parameter correlating the shear layer growth rate with compressibility effects is the convective Mach number, defined for the mixing of two streams of the same gas as [3]

$$M_c = \frac{u_1 - u_2}{c_1 + c_2} \tag{1}$$

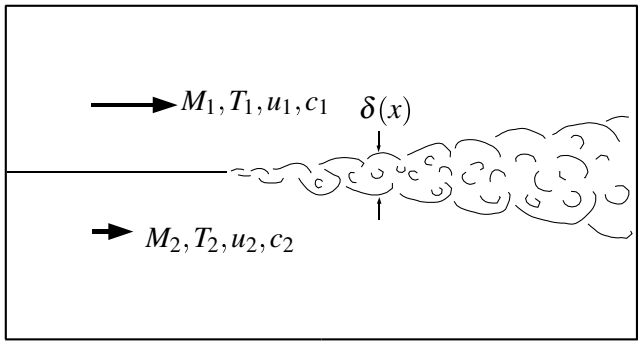

Fig. 1 Flow configuration for the free shear layer.

where u is the streamwise velocity and c is the speed of sound. In general, an increase in the convective Mach number leads to a decrease in the shear layer growth rate for fixed velocity ratio $r = u_2/u_1$ and density ratio $s = \rho_2/\rho_1 = T_1/T_2$. This is usually characterized by the compressibility factor Φ, defined as the ratio of the compressible growth rate to the incompressible growth rate at the same velocity and density (or temperature) ratios:

$$\Phi = \frac{(\mathrm{d}\delta/\mathrm{d}x)_c}{(\mathrm{d}\delta/\mathrm{d}x)_i} \tag{2}$$

More detailed discussion of compressibility effects in turbulent free shear layers can be found in Lele [4] and Smits and Dussauge [5].

Experimental Data

Collection of validation data is closely related to the first two steps of the validation process outlined in the Introduction: namely, consistent specification of the SRQ used for the comparison of computation and experiment, and careful postprocessing of the experimental data. In the case of a validation experiment, the experiment and computation can (ideally) be constructed so that consistency in boundary conditions, flow conditions, etc., are strictly maintained. In the present case we are examining a wide range of sources for experimental data in an attempt to find a consistent group of experiments that can be used for validation. Possible inconsistencies can arise in, for example, specification of the SRQ, postprocessing of experimental measurements, boundary conditions, or wind tunnel noise issues. Definitive validation results depend on the ability to identify and eliminate most or all of these inconsistencies. On the other hand, the largest possible ensemble of consistent data is desired because the level of confidence in the data increases with the number of independent measurements.

Experimental data on high-speed shear layers are available from a number of independent sources. Many researchers continue to use the "Langley curve" [6] as a data set to validate and calibrate turbulence models. We note that the data used to construct the Langley curve were all measured before 1970, suggesting that perhaps there is a need for an updated "recommended data set." The total collection of available experimental investigations employs a wide range of diagnostic techniques within many distinct facilities. Comparisons of data for the compressibility factor obtained over a range of convective Mach numbers from various experiments seem to indicate a significant spread in the data (see, e.g., Lele [4]). Other presentations of data from multiple sources appear in [7–11]. These five sources of compiled shear layer data form the starting point for the present compilation.

This data set was first filtered by eliminating results obtained by estimating a growth rate based on pitot pressure thickness or the visual thickness from an optical photograph. Thickness based on pitot pressure and optical photographs give results that differ significantly from those obtained using a velocity layer thickness definition. In particular, the Φ versus M_c distribution for pitot/optical thickness data falls more rapidly with increasing M_c and converges to a lower asymptote of Φ for high M_c. An example of this behavior is given in Figs. 16 and 17 of [11]. A common assumption is that the Φ versus M_c curve is universal and independent of the definition of the mixing layer thickness. For this to be true, the ratio of the growth rate measured using one thickness definition to that using a different definition must be a constant that does not depend on the velocity ratio, density ratio, and convective Mach number. This assumption requires definitive examination of multiple data sources and, to our knowledge, this has not yet been carried out in a systematic fashion. We do not seek to accomplish this here, but rather choose a consistent framework for the analysis by considering only experimental measurements of mixing layer thickness based on measured velocity profiles. Other sources of data, such as the original data presented in [7], are not used due to doubts as to whether the mixing layers considered were fully developed (and, therefore, self-similar).

The remaining data are analyzed using a consistent method to estimate the compressibility factor Φ given the experimental flow conditions for each experiment considered. First, a consistent

method for determining the relevant incompressible growth rate $(\mathrm{d}\delta/\mathrm{d}x)_i$ for each experimental data point is required. The compressible growth rate is then determined from the reported experimental data based on the same thickness definition used to calculate the incompressible growth rate.

The incompressible growth rate is a function of the thickness definition, the velocity ratio $r = u_2/u_1$, and the density ratio $s = \rho_2/\rho_1$. We consider several of the more popular thickness definitions based on measurements of the velocity profile that have been used in the literature. The energy thickness δ_s, or $\sqrt{10}\%$ velocity thickness, is defined later on in Eq. (10). Other experimental results are reported in terms of the 10% velocity thickness δ_b [remove the exponents of 2 in (10)], and the vorticity thickness $\delta_\omega = (u_1 - u_2)/(\partial u/\partial y_{\max})$. Regardless of the thickness definition, analysis of the incompressible velocity profile [12] (see p. 737) leads to the following similarity profile:

$$\frac{u - u_2}{u_1 - u_2} = \frac{1}{2}[1 + \mathrm{erf}(\eta)], \qquad \eta = \frac{\sigma y}{x}, \qquad \sigma = \sigma_0/\lambda_s \tag{3}$$

where approximate theoretical arguments (see Brown [13] and Papamoschou and Roshko [11]) give

$$\lambda_s = \frac{(1 - r)(1 + \sqrt{s})}{2(1 + r\sqrt{s})} \tag{4}$$

Note that σ_0 is an empirical constant. There is a general lack of consensus on the appropriate value for σ_0. Birch and Eggers [6] present the spreading parameter σ_0 from 11 subsonic experiments. The average value of all of the spreading parameters is 11.2 whereas an average of the more reliable data gives $\sigma_0 = 11.0$. Schetz [14] also recommends the value $\sigma_0 = 11.0$ on p. 381 of his text, based on relatively recent data. These considerations led to the choice of $\sigma_0 = 11$ for the present analysis.

Given the error function velocity profile, the mixing layer thickness definitions, and the chosen value of σ_0, the following relations hold for the incompressible growth rate:

$$\frac{\mathrm{d}\delta_{b_i}}{\mathrm{d}x} = C_b\lambda_s, \qquad \frac{\mathrm{d}\delta_{s_i}}{\mathrm{d}x} = C_s\lambda_s, \qquad \frac{\mathrm{d}\delta_{\omega_i}}{\mathrm{d}x} = C_\omega\lambda_s \tag{5}$$

where the constants in (5) are given by

$$C_b = 0.165, \qquad C_s = 0.136, \qquad C_\omega = 0.161 \tag{6}$$

An alternative correlation [15] uses the hyperbolic tangent velocity profile,

$$\frac{u - u_2}{u_1 - u_2} = \frac{1}{2}[1 + \tanh(\eta)], \qquad \eta = \sigma(y - y_0)/x \tag{7}$$

Here y_0 is the centerline of the mixing layer, defined as the y coordinate where $u = (u_1 + u_2)/2$. This profile leads to alternative expressions for the incompressible spreading rate:

$$\frac{\mathrm{d}\delta_{b_i}}{\mathrm{d}x} = E_b\lambda_s, \qquad \frac{\mathrm{d}\delta_{s_i}}{\mathrm{d}x} = E_s\lambda_s, \qquad \frac{\mathrm{d}\delta_{\omega_i}}{\mathrm{d}x} = E_\omega\lambda_s \tag{8}$$

where

$$E_b = 0.200, \qquad E_s = 0.168, \qquad E_\omega = 0.182 \tag{9}$$

The present approach first determines the flow conditions from the experimental description, which gives the Mach numbers M_1 and M_2, velocity ratio r, and density ratio s for the two layers. Then, the convective Mach number and the velocity-density parameter λ_s are determined from (1) and (4), respectively. The experimental growth rate of the compressible mixing layer is obtained from tabulated data or figures given in each of the original papers. The incompressible mixing layer growth rate is calculated based on the same definition of the mixing layer thickness, and one of the two assumed velocity profiles, (3) or (7). The compressibility factor is then computed from Eq. (2). The error function correlation results given in Eq. (5) are used for the calculation of the incompressible growth rates for all cases except for the data of [15,16], which used the hyperbolic tangent correlation to collapse the compressible shear layer data. The consistent approach for their data is to use the hyperbolic tangent profile results of Eq. (8) to also compute the incompressible growth rate.

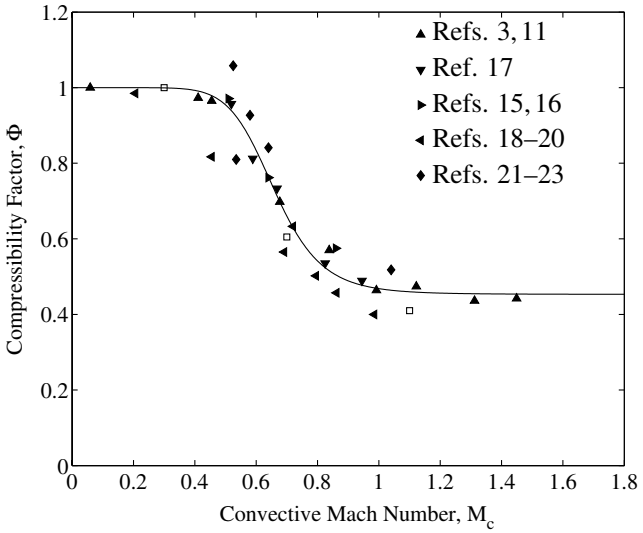

Fig. 2 Experimental data for compressibility factor versus convective Mach number. The open squares are DNS results [24] for $s = 1$. The solid line is the regression fit of Eq. (17).

The resulting ensemble of data [3,11,15–23] is presented in Fig. 2 and shown in Table 1. These data are organized into groups of sources, some of which are themselves compilations of results from several experiments. The experimental result of Chinzei et al. [17] at $M_c = 0.270$, $\Phi = 1.35$ has been omitted from the recommended data set as it appears to be in error. A possible source of the error for this data point may be the presence of pressure waves and/or freestream turbulence in the secondary stream, visible in Schlieren images presented in [17]. Further justification for elimination of this data point is that it is the only condition considered by [17] with $M_2 > 1$. The direct numerical simulation (DNS) results of Pantano and Sarkar [24] for a temporally developing compressible mixing layer are also presented in the figure, and they compare very favorably to the assembled experimental data.

The similarity region growth rate of a compressible free shear layer is not uniquely defined by convective Mach number alone. The definition of the shear layer also depends on the ratios of static and total temperature from one uniform stream to the other. Although most experimental evidence suggests compressibility effects in turbulent shear layers are well correlated by convective Mach number alone, computational models may give predictions for compressibility factor that are not universal, also depending on static and/or total temperature ratios (see, e.g., Zeman [25]). These

Table 1 Recommended shear layer experimental data

Ref.	M_c	Φ	Ref.	M_c	Φ
[3,11]	0.059	1.000	[15]	0.51	0.971
[3,11]	0.411	0.973	[15]	0.64	0.762
[3,11]	0.455	0.965	[16]	0.86	0.575
[3,11]	0.677	0.698	[18,19]	0.206	0.985
[3,11]	0.838	0.570	[18,19]	0.455	0.817
[3,11]	0.992	0.464	[18,19]	0.691	0.565
[3,11]	1.122	0.474	[18,19]	0.720	0.633
[3,11]	1.312	0.436	[20]	0.795	0.502
[3,11]	1.449	0.442	[18,19]	0.862	0.457
[17]	0.270	1.350	[18,19]	0.985	0.400
[17]	0.519	0.957	[21]	0.525	1.058
[17]	0.589	0.812	[21]	0.535	0.810
[17]	0.668	0.733	[22]	0.580	0.927
[17]	0.825	0.535	[21]	0.640	0.841
[17]	0.945	0.489	[22,23]	1.040	0.518

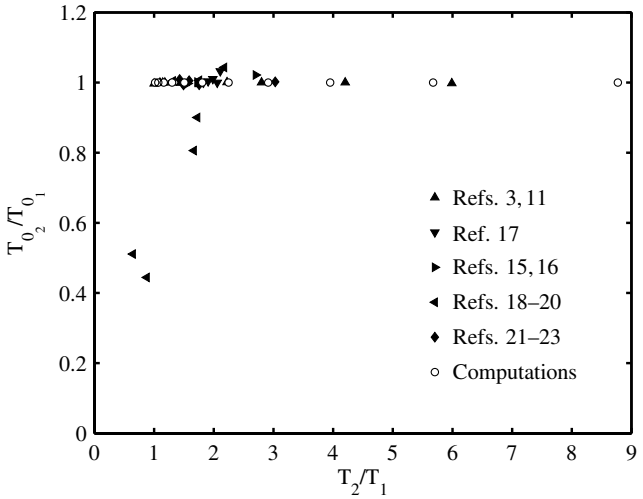

Fig. 3 Total temperature ratio versus static temperature ratio for the experimental data set and for the computations.

parameters should be chosen for the computational study by appealing to the range of values present in the experiments, allowing for maximum consistency between computation and experiment. Figure 3 shows the total and static temperature ratios for the experimental data set. Most of the experiments were conducted at constant total temperature T_0, with the exception of a few cases from the work of Goebel and Dutton [18]. The present computations, to be discussed in the next section, were therefore carried out for shear layers with $T_{0_2}/T_{0_1} = 1$.

Computational Models

Most two-equation turbulence models in their original form do not correctly predict the significant decrease in the mixing layer growth rate with increasing convective Mach number, necessitating inclusion of a compressibility correction. Development of compressibility corrections was an active research area in the early 1990s, leading to the introduction of several widely referenced models. These include the class of "dilatation-dissipation" models developed by Sarkar et al. [26], Zeman [25], and Wilcox [27]. Compressible dissipation terms appearing in the turbulence kinetic energy equation are modeled based on a local turbulence Mach number ($M_t = \sqrt{2k/c^2}$), leading to a reduction in turbulence levels and, consequently, in mixing layer growth rate. The correction of Sarkar et al. [26], called here the "Sarkar" correction, is based on the observation that the compressible, or dilatation, dissipation varies on a time scale that is fast relative to the incompressible, or solenoidal, dissipation. This leads to the conclusion that the dilatation dissipation increases with increasing convective Mach number. The Zeman correction, on the other hand, is based on the assumption that eddy shocklets are the primary mechanism for the observed decrease in growth rate. Wilcox's correction does not introduce any new physical modeling and is very similar in functional form to the first two models with a slight modification to mitigate inaccuracy in skin friction predictions of the former models.

The dilatation-dissipation models were developed at a time when the understanding of compressible turbulence in free shear layers was relatively unclear. Since then, DNS of high-Reynolds number compressible mixing layers [24,28,29] have revealed that the primary mechanism of reduction in the growth rate is decreased turbulent production resulting from decrease in the pressure-strain correlation term of the Reynolds stress equation, whereas the dilatational terms were shown to be small. Thus, the compressibility corrections based on the dilatation-dissipation term are not grounded in the relevant physics. It is not the authors' intent to advocate the use of these compressibility corrections; rather, they serve as a useful proxy to demonstrate the validation process. Further, providing a detailed study of their performance provides error bounds for those engineers currently using such models. Despite the popularity of these compressibility corrections, only limited independent tests of their performance have been published. Some comparisons of model performance were made in the open literature [30,31], but these were not particularly complete tests, and the conclusions suffered from a general lack of confidence in the experimental data set. Future validation studies should focus on the more recent pressure-strain modeling concepts; see, e.g., Adumitroaie et al. [32] and Aupoix [33].

Table 2 Flow parameters for the shear layer computations

M_c	M_1	M_2	T_2/T_1	u_2/u_1
0.10	0.3016	0.1	1.0162	0.3342
0.24	0.5913	0.1	1.0678	0.1747
0.38	0.8966	0.1	1.1585	0.1200
0.52	1.2264	0.1	1.2982	0.0929
0.66	1.5920	0.1	1.5039	0.0770
0.80	2.0086	0.1	1.8033	0.0669
0.94	2.4976	0.1	2.2431	0.0600
1.08	3.0914	0.1	2.9055	0.0551
1.22	3.8411	0.1	3.9429	0.0517
1.36	4.8343	0.1	5.6628	0.0492
1.50	6.2347	0.1	8.7568	0.0475

In this work we consider validation of the three mentioned dilatation-dissipation models when implemented as a correction to either the standard k–ε model [34] with the low-Reynolds number modification of Nagano and Hishida [35], or the Wilcox (1998) k–ω [30] turbulence model. Note that the present study is concerned with validation of the models for mixing layer flows only; a complete analysis would necessarily include a number of wall-bounded flow cases. The k–ε model equations and constants are given by the compressible form of Eqs. (4.46)–(4.49) in Wilcox [30]. The k–ω model is given by the compressible form of Eqs. (4.36)–(4.42) in Wilcox [30]. The implementation of the compressibility corrections is given by Eqs. (5.62)–(5.65) and Eqs. (5.70)–(5.73) in the same reference. The recommended values of $\Lambda = 0.60$ and $M_{to} = 0.10\sqrt{2/\gamma + 1}$ for free shear flows were used in the Zeman model.

The first turbulence model considered was the k–ε model with the Zeman compressibility correction. This model was examined using the SACCARA finite volume code (described below), which solves the Favre-averaged Navier–Stokes equations. Detailed solution verification was performed for this case and is described in the following discussion. This first case demonstrates the necessary steps for model validation, including prerequisite solution verification exercises. The other turbulence model/correction combinations were examined using the MIXER similarity solution code developed by Wilcox [30]. The MIXER code computes a shear layer similarity solution for the turbulence model of interest assuming 1) the effects of laminar viscosity are negligible and 2) there exists zero pressure gradient. This second methodology allowed for more economical comparison of the different models, resulting in a more comprehensive study of available models. The close similarity of the full CFD solutions to the similarity solutions will be demonstrated later for the k–ε/Zeman model, justifying the use of the similarity code for model validation.

Table 2 gives the flow parameters for the set of 11 shear layers computed in this study. The medium for all the computations is air, modeled as an ideal gas. This set of parameters spans the convective Mach number range of the experimental data, from 0 to 1.5.

Finite Volume Solutions with the k–ε/Zeman Model

The k–ε/Zeman solutions were computed using the SACCARA (Sandia Advanced Code for Compressible Aerothermodynamics Research and Analysis) code [36,37], which employs a block-structured, finite volume discretization method. The numerical fluxes are constructed with the symmetric total variation diminishing (TVD) scheme of Yee [38], which gives a second order theoretical asymptotic spatial convergence rate in smooth flow regions. The minmod limiter is applied to enable robust computation of shocks

and contact discontinuities. The equations are advanced to steady state using the lower–upper symmetric Gauss–Seidel (LU-SGS) scheme of Yoon and Jameson [39]. Solutions were considered iteratively converged when the L_2 norm of the momentum equation residuals decreased 8 orders of magnitude.

In the computations, the splitter plate is assumed to have zero thickness, with no-slip and adiabatic wall boundary conditions applied on the plate surface (Fig. 4). The inflow above and below the plate is specified as uniform and normal to the inflow boundary, which is located 1 m upstream of the splitter plate trailing edge. Turbulent boundary layers develop along the plate before separating at the trailing edge to form the mixing layer. For supersonic inflow, all flow properties are specified, whereas for subsonic inflow the total pressure, total temperature, and flow angle are specified. Uniform inflow profiles of k and ε were specified such that $\mu_T = \mu$, where $\mu_T = 0.09\rho k^2/\varepsilon$, and $k = 1.2 \times (0.01u)^2/2$.

The top and bottom walls, which are modeled as free-slip boundaries, are placed far from the shear layer at $y = \pm 2$ m to minimize the generation of an artificial pressure gradient in the x direction. Turbulent shear layer development and growth rates can be influenced by the presence of pressure gradients set up in a wind tunnel or by a finite computational domain size. The main cause of the pressure gradient is the acceleration of the flow outside of the shear layer necessary to ensure mass conservation as the region of low momentum fluid within the shear layer expands. For typical experimental configurations the maximum mean pressure deviation along the wind tunnel test section walls is about 6% [15,18]. The pressure gradients set up in the computations are observed to increase as the convective Mach number is increased. However, the maximum computed deviation in pressure near the shear layer (measured along the line $y = 0$) is only 0.3% for $M_c = 1.50$. Thus, the effect of the pressure gradient on the growth rate is expected to be very small.

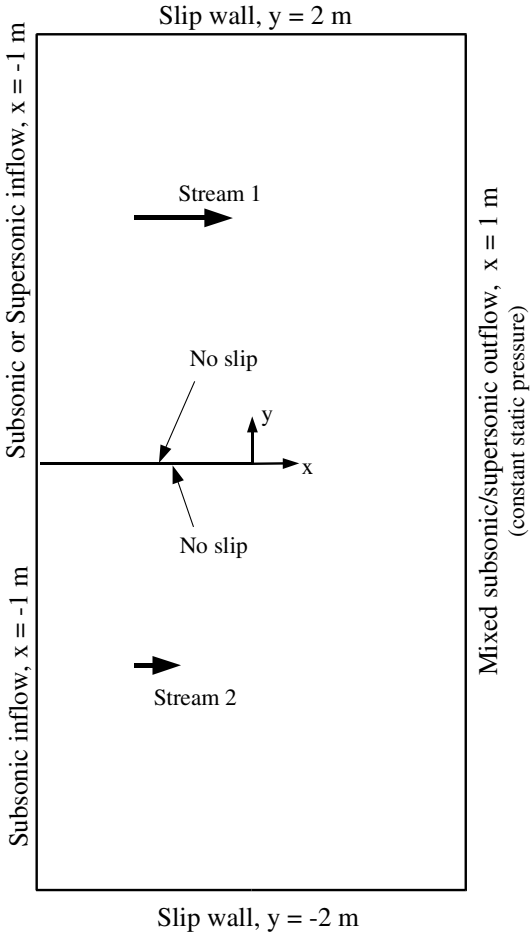

Fig. 4 Schematic of the shear layer computational domain.

The outflow boundary is located 1 m downstream of the splitter plate trailing edge. A simple extrapolation boundary condition is applied at points on the outflow where the flow is locally supersonic, whereas a characteristic-based boundary condition with specified outflow pressure is applied at subsonic points. The specified pressure for the subsonic outflow boundary cells is set equal to the inflow static pressure, consistent with the assumption of the negligible streamwise pressure gradient.

For each convective Mach number, solutions were calculated on three grids: a coarse, medium, and fine grid. Beginning with the fine grid, each successively coarser grid is obtained by removal of every other grid line (in each spatial dimension) from the previous grid. The resulting grid sizes are given in Table 3; the same three grids were used for each set of flow parameters. The grids are uniform in the streamwise, or x, direction, and stretched in the cross stream, or y direction, so that grid cells are clustered within the shear layer. The cells are highly clustered in the y direction near the trailing edge and become less clustered with increasing x to account for the shear layer growth. The minimum transverse grid spacing at the trailing edge is labeled Δy_1 and the minimum spacing at the outflow boundary is Δy_2. Table 3 includes values for these two grid spacings for each grid. The number of grid points across the shear layer is a useful metric for grid resolution. The $M_c = 1.50$ shear layer had the lowest growth rate and the thinnest shear layer near the outflow boundary. For this case, the shear layer at $x = 0.9$ m was resolved by about 37 points on the coarse grid and by about 141 points on the fine grid.

Postprocessing Procedures

For postprocessing of the computational results we use the energy thickness definition for the mixing layer [40]

$$\delta_s = y_1 - y_2$$

$$y_1 \text{ is the location where } \frac{(u-u_2)^2}{(u_1-u_2)^2} = 0.9$$

$$y_2 \text{ is the location where } \frac{(u-u_2)^2}{(u_1-u_2)^2} = 0.1 \tag{10}$$

where u is the mean streamwise velocity. As we have already mentioned, the thickness grows linearly with x only for large x due to the presence of the development region that precedes the similarity region. This behavior is depicted for the $M_c = 0.80$ case in Fig. 5. Given that the growth rate actually approaches a constant value only asymptotically, the thickness distribution is fit with a curve that mimics this functional form. The function used for the fit is

$$\delta_s(x) = \beta_0 + \beta_1 x + \beta_2 x^{-1} \tag{11}$$

which leads to a growth rate that approaches β_1 as x becomes large. The coefficient β_1 is taken to be the actual fully developed shear layer growth rate.

Examination of all the computational results reveals a short region near the outflow boundary that shows a slight influence of the computational boundary conditions. The outflow boundary condition assumes a locally uniform flow and thus generates some error when shear is present at the boundary. This error propagates back into the computational domain, with the largest influence on the solution occurring within 0.05 m of the boundary. To minimize the effect of the outflow boundary error and the development region, the region used for the thickness distribution curve fit, Eq. (11), was $0.5 \le x \le 0.9$ m for all the calculations.

Table 3 Grid parameters for the shear layer computations

Grid	N_i	N_j	Δx $\times 10^{-3}$ m	Δy_1 $\times 10^{-6}$ m	Δy_2 $\times 10^{-6}$ m
Coarse	150	68	6.67	2.05	202
Medium	300	134	3.33	1.0	100
Fine	600	268	1.67	0.5	50

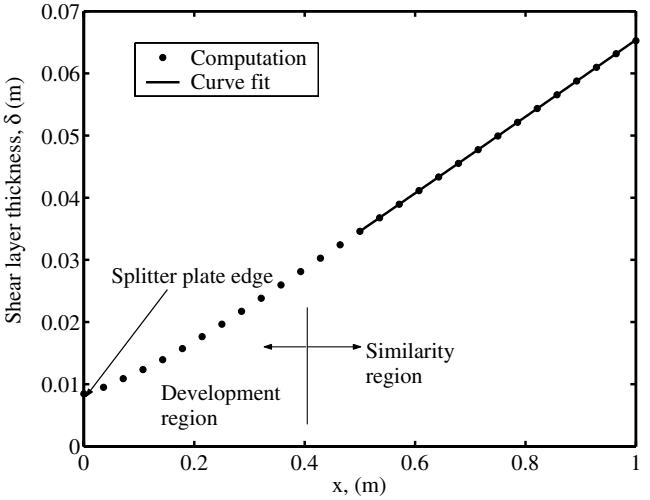

Fig. 5 Computed shear layer thickness for $M_c = 0.80$ (medium grid result, every tenth point plotted), along with the curve fit computed from data in the range $0.5 \leq x \leq 0.9$ m.

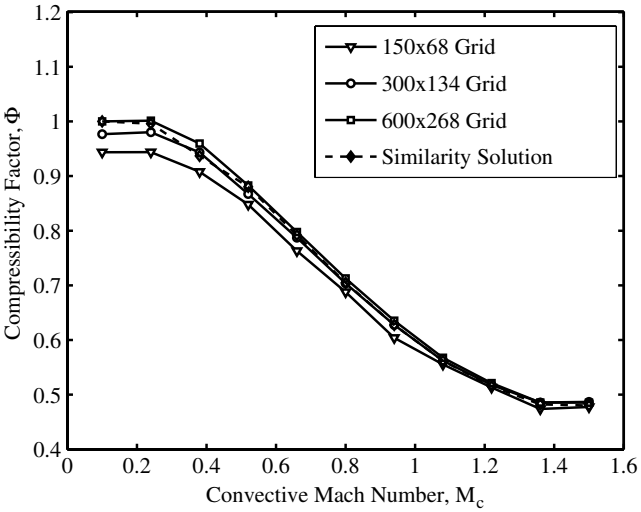

Fig. 6 Grid convergence study results for the k–ε/Zeman shear layer computations, with comparison to the similarity solution of Wilcox [30].

Table 4 Fine grid computational results, k–ε/Zeman model

M_c	$(\frac{d\delta}{dx})_i$	$(\frac{d\delta}{dx})_c$	Φ
0.10	0.0514	0.0514	1.0000
0.24	0.0711	0.0712	1.0014
0.38	0.0792	0.0760	0.9596
0.52	0.0836	0.0738	0.8828
0.66	0.0865	0.0690	0.7977
0.80	0.0884	0.0630	0.7127
0.94	0.0894	0.0568	0.6353
1.08	0.0895	0.0508	0.5676
1.22	0.0873	0.0455	0.5212
1.36	0.0838	0.0407	0.4857
1.50	0.0756	0.0367	0.4854

Following extraction of the compressible growth rate $(d\delta/dx)_c$, the incompressible growth rate $(d\delta/dx)_i$ must be evaluated at the same velocity and temperature ratios. Incompressible or nearly incompressible results are difficult to obtain with a compressible CFD code. Therefore, the incompressible growth rate was obtained by computing a similarity solution for the given turbulence model and flow conditions; details of the similarity solution are given in the next section. In Table 4, the computed fine grid results for compressible growth rate are given with the corresponding incompressible growth rate and the resulting compressibility factor. Utilizing the validation terminology of [1,2], the SRQ of interest is the compressibility factor Φ.

Solution Verification

Before validation activities, it is necessary to estimate the level of numerical error present in the computed SRQ through solution verification exercises. Two types of verification efforts were conducted for this problem: 1) comparison to an available similarity solution, and 2) estimation of grid convergence error in the SRQ of interest. The similarity solution is derived by Wilcox [30] in his turbulence modeling text and implemented in the MIXER code that is distributed with the text. The similarity solution is computed using the same turbulence model and compressibility correction as the Navier–Stokes calculations, but under the assumptions of negligible laminar viscosity and an asymptotic state attained far downstream. The governing equations are first transformed to a similarity form before application of a second transformation devised by Rubel and Melnik [41] that removes certain numerical difficulties. The equations are advanced in time using a Crank–Nicholson scheme with second order spatial differencing.

Initial comparisons of the computed Favre-averaged Navier–Stokes solutions and the similarity solution showed differences of 10–15% in the growth-rate predictions for $M_c > 1$. This led to the discovery of a coding error in the MIXER code. Specifically, a turbulent transport term had been inadvertently left out of the mean energy equation.[§] This experience illustrates the importance of code verification, in addition to solution verification, efforts as a precursor to validation studies. Following correction of the error in the similarity code, the Navier–Stokes results on the fine grid compared very well to the similarity solution, as shown in Fig. 6. Note that code-to-code comparisons such as this one are no substitute for more rigorous code verification methods [42], although in this case the comparison served as a useful confidence-building and error discovery exercise.

Further confidence in the numerical solutions comes from estimates of spatial discretization error. An attempt was made to estimate the actual order of convergence using the three CFD solutions and Richardson extrapolation formalism [42,43]. This effort was not successful, most likely due to some combination of nonasymptotic error behavior, ill-behaved error terms in the shock-capturing scheme, and postprocessing errors associated with extraction of the mixing layer growth rate. Roache [42] describes how an estimated fractional error can be used to consistently report grid convergence results when there is some doubt about the validity of Richardson extrapolation. The estimated fractional error for the fine grid solution is given by

$$\varepsilon_1 = \frac{|(d\delta/dx)_1 - (d\delta/dx)_2|/(d\delta/dx)_1}{r^p - 1} \tag{12}$$

where the subscript 2 denotes the medium grid solution, and the subscript 1 the fine grid solution. Here we assume either $p = 2$, according to the theoretical asymptotic spatial convergence rate of the finite volume scheme, or $p = 1$, for a "worst case" scenario of first order convergence.

Figure 7 compares the estimated fractional error in the compressible shear layer growth-rate computation, assuming $p = 1$ or $p = 2$. The estimated error is less than 2.5% for $p = 1$ and less than 1% for $p = 2$ over the entire range of convective Mach number. We also note that the fine grid result is within 1.5% of the similarity solution over the range of convective Mach number considered. Likely sources of this slight discrepancy, beyond the fine grid discretization error, include the effects of mild pressure gradients present in the Navier–Stokes computations, absence of laminar viscosity in the similarity solutions, and biases introduced by the postprocessing procedure used to extract the growth rate. Given the estimated error together with the proximity of the fine grid solution to

[§]Wilcox was informed of the error and he responded that it would be corrected in future editions of the text and noted on his web site www.dcwindustries.com (private communication, March 2004).

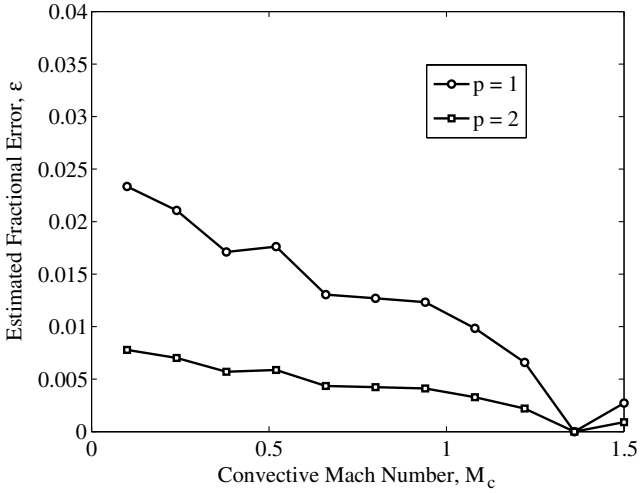

Fig. 7 Estimated fractional error in the compressible mixing layer growth rate for the fine grid solution assuming $p = 1$ and $p = 2$.

the similarity solution, we estimate the error bound for the fine grid solution to be approximately 2%. This is deemed to be an acceptable error level for validation of the model; indeed, the modeling error turns out to be significantly larger than the estimated numerical error as discussed in the next section.

Similarity Solutions

The remainder of the turbulence models were computed using the MIXER code. The transformed similarity relations form a two-point boundary value problem that is solved iteratively on a one-dimensional grid that spans the mixing layer. The similarity solution calculations were considered grid/iteratively converged after the first three significant digits of the predicted shear layer growth rate were unchanged with further grid refinement/iteration. The predicted compressibility factors for all the models considered are compared to the experimental data set in Fig. 8. There is significant spread in the model predictions, even much more than the experimental data. Although it is clear from the figure that some of the models are inferior to others, it is difficult to pick a "best" model. The usual practice in model validation is to stop here and make qualitative statements based on the appearance of agreement in the plot. The following section examines model performance quantitatively through the use of a validation metric.

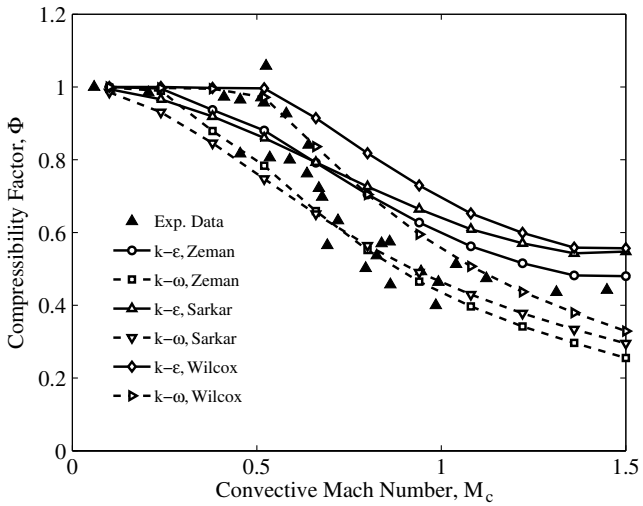

Fig. 8 Model prediction of compressibility factor compared with the experimental data.

Application of the Validation Metric

Confidence Intervals and Model Comparisons

Of central importance to construction of the validation metric described in Oberkampf and Barone [1,2] is the calculation of simultaneous confidence intervals about the estimated mean of the experimental data. The estimated mean represents the true system response over a range of the input parameter(s), as best can be known from the experimental measurements. The confidence intervals provide an estimate of the experimental uncertainty at a given level of confidence. Thus the outcome of the validation metric methodology includes an estimate of the modeling error, a statement of the uncertainty in the experimental data, and a confidence level for the specified experimental uncertainty.

Suppose the data set is described by n measurements of a SRQ denoted by y_e^i, which is a function of a single independent experimental variable x. In our case the independent variable is the convective Mach number M_c and the SRQ is the compressibility parameter Φ. Assume that the mean of the data is described by a nonlinear regression fit of the form $\bar{y}_e = f(x; \boldsymbol{\theta})$, where $\bar{y}_e$ is the estimated mean and $\boldsymbol{\theta}$ is the p-dimensional vector of regression parameters. The error sum of the squares of the regression fit is

$$S(\boldsymbol{\theta}) = \sum_{i=1}^{n} [y_e^i - f(x_i; \boldsymbol{\theta})]^2 \tag{13}$$

As discussed in [1,2], the $1 - \alpha$ quantile confidence intervals about the estimated mean may be computed by solving an inequality for the set of $\boldsymbol{\theta}$ that satisfies

$$\boldsymbol{\theta}, \qquad \text{such that } S(\boldsymbol{\theta}) \le S(\hat{\boldsymbol{\theta}}) \left[1 + \frac{p}{n-p} F(p, n-p, 1-\alpha) \right] \tag{14}$$

Here $F(\nu_1, \nu_2, 1 - \alpha)$ is the F probability distribution, ν_1 and ν_2 are the 2 degree-of-freedom parameters, and $\hat{\boldsymbol{\theta}}$ is the least squares regression parameter vector. The confidence intervals are obtained by computing the envelope of regression function curves evaluated for all $\boldsymbol{\theta}$ satisfying Eq. (14).

Before the validation metric result can be computed, one must prescribe a form for the nonlinear regression fit to the experimental data presented in Fig. 2. It is important that the proper functional behavior of the data, either established through theoretical derivation or deduced from the trend in experimental measurements or reliable DNS, should be reflected in the regression function form. For the compressible shear layer we know that Φ must equal unity in the incompressible limit $M_c \to 0$. Results from DNS combined with supporting analysis suggest that $\Phi \to$ const as M_c becomes large [24]. These considerations lead to the following choice of regression function, taken from Paciorri and Sabetta [44]:

$$\Phi(M_c, \hat{\boldsymbol{\theta}}) = 1 + \hat{\theta}_1 \left(\frac{1}{1 + \hat{\theta}_2 M_c^{\hat{\theta}_3}} - 1 \right) \tag{15}$$

The proper incompressible limit is recovered and examination reveals the desired behavior for large M_c:

$$\lim_{M_c \to \infty} \Phi = 1 - \hat{\theta}_1 \tag{16}$$

The Matlab function nlinfit is used to calculate the following regression coefficients for the experimental data set:

$$\hat{\theta}_1 = 0.5468, \qquad \hat{\theta}_2 = 35.53, \qquad \hat{\theta}_3 = 8.614$$

We now choose to evaluate the modeling error relative to 90% confidence intervals on the experimental data. The model error is defined as the difference between the model prediction y_m and the estimated mean of the experimental data $\bar{y}_e$. The model errors for the models based on the k–ε model are shown in Fig. 9, whereas the error for the k–ω models is shown in Fig. 10. The deviations of the 90% confidence intervals from the estimated mean are also pictured in both figures. This type of plot gives the analyst a feel for the accuracy

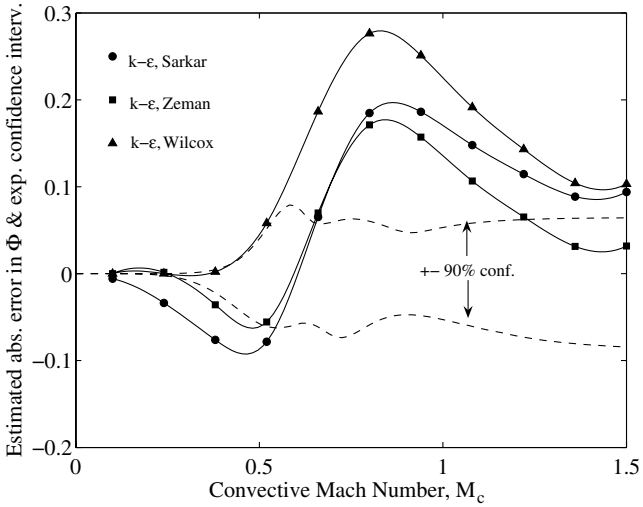

Fig. 9 Validation metric result and 90% confidence interval for Φ, *k–ε* models.

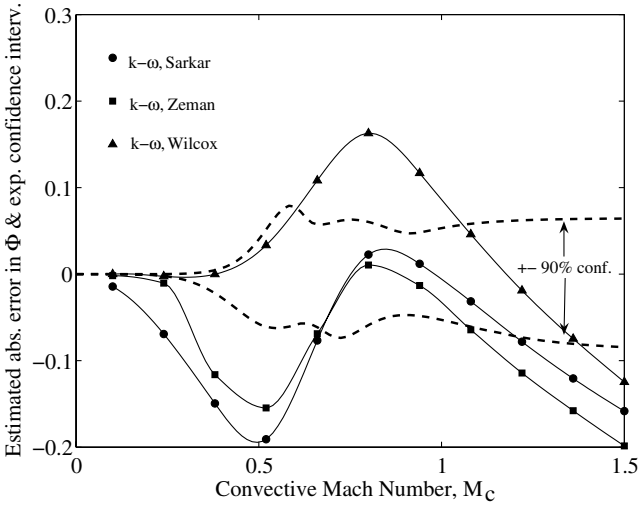

Fig. 10 Validation metric result and 90% confidence interval for Φ, *k–ω* models.

of the model for particular values of the input parameter, as well as information provided by the confidence interval width regarding the confidence that the estimated experimental mean is a good measure of the true experimental mean at a particular input parameter value. Good model performance relative to an experimental data set is indicated by the estimated model error falling well within the confidence intervals.

The first observation of model performance based on these results is that none of the models performs uniformly well across the entire range of convective Mach number. The precision of evaluating models using the validation metric approach can be clearly seen by comparing Figs. 9 and 10 versus Fig. 8. The Wilcox compressibility correction gives good results for both turbulence models for $M_c < 0.5$, a consequence of the higher turbulence Mach number threshold used by this correction. Both the Sarkar and Zeman corrections overpredict the decrease in Φ at low convective Mach number, especially when used with the *k–ω* model. Over the range $0.5 < M_c < 1.3$, all corrections overpredict the turbulent mixing when applied to the *k–ε* model. The *k–ω*/Wilcox model also underpredicts the sharp drop in Φ, but to a lesser degree and over a shorter range of M_c. Although the *k–ω* model with the Zeman and Sarkar corrections gives good agreement over the range $0.7 < M_c < 1.1$, the trend of these models does not match the trend of the data.

The model behavior for $M_c > 1.2$ appears to depend more strongly on the base turbulence model rather than on the compressibility correction. The *k–ε* results pictured in Fig. 9 show the error leveling off for large M_c, due to the associated asymptotic behavior of the model shown in Fig. 8. Contrast this with the behavior of the *k–ω* model in Fig. 10, where the error continues to increase with increasing M_c due to a continued decrease in Φ. The high M_c model behavior is apparently dominated by the turbulence model prediction of *incompressible growth rate* as a function of the density ratio. For the present cases, the density ratio s decreases with increasing M_c. For all models with all compressibility corrections, the compressible growth rate decreases monotonically for large M_c. The turbulence model predictions (as computed by the MIXER code) for incompressible growth rate versus density ratio are compared to the theoretical relation, Eq. (5), in Fig. 11. The flow conditions for the points computed in Fig. 11 are identical to those listed in Table 2. The *k–ω* incompressible growth rate is fairly constant at low density ratio, leading to the observed further decrease in Φ. In contrast, the *k–ε* incompressible growth rate decreases at low density ratio, in better agreement with the approximate theory.

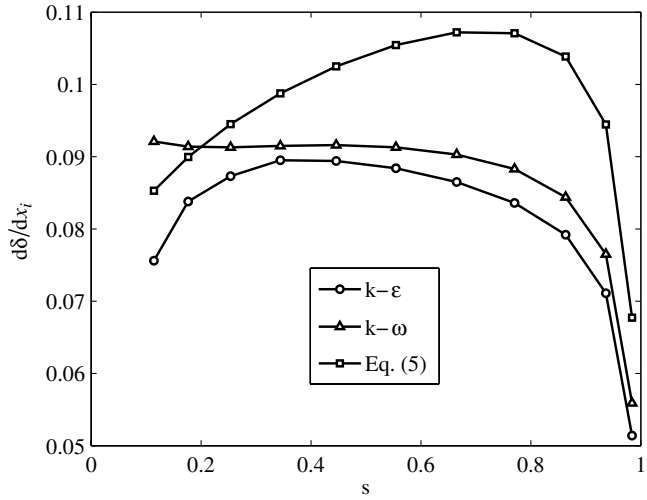

Fig. 11 Model prediction of incompressible growth rate versus density ratio.

Global Validation Metrics

Model accuracy can be summarized in a compact and quantitative form by definition of an appropriate *global validation metric* [1,2]. Global metrics are constructed by considering norms of the error in the models relative to the estimated mean of the experimental data. The following L_1 norm is useful to interpret the estimated average relative error of the model result $y_m(x)$ over the range of the data $x_l \le x \le x_u$:

$$\left|\frac{\tilde{E}}{\bar{y}_e}\right|_{\text{avg}} = \frac{1}{x_u - x_l}\int_{x_l}^{x_u}\left|\frac{y_m(x) - \bar{y}_e(x)}{\bar{y}_e(x)}\right| \mathrm{d}x \tag{17}$$

For situations where there may be a large error over a small range of the data, it is useful to define a maximum absolute relative error using the L_∞ norm

$$\left|\frac{\tilde{E}}{\bar{y}_e}\right|_{\max} = \max_{x_l \le x \le x_u}\left|\frac{y_m(x) - \bar{y}_e(x)}{\bar{y}_e(x)}\right| \tag{18}$$

These quantitative measures of agreement are incomplete without comparison to the degree of confidence in the experimental data. The average width of the confidence interval normalized by the absolute value of the estimated experimental mean over the range of the data is

$$\left|\frac{CI}{\bar{y}_e}\right|_{\text{avg}} = \frac{1}{x_u - x_l}\int_{x_l}^{x_u}\left|\frac{y^+_{CI}(x) - y^-_{CI}(x)}{2\bar{y}_e(x)}\right| \mathrm{d}x \tag{19}$$

$|CI/\bar{y}_e|_{\text{avg}}$ provides a quantity with which to interpret the significance of $|\tilde{E}/\bar{y}_e|_{\text{avg}}$. The significance of $|\tilde{E}/\bar{y}_e|_{\max}$ is evaluated

Table 5 Relative error in compressibility factor prediction

Turb. Model	Comp. Corr.	$\lvert\frac{\bar{E}}{\bar{y}_e}\rvert_{\text{avg}}$ %	$\lvert\frac{\bar{CI}}{\bar{y}_e}\rvert_{\text{avg}}$ %	$\lvert\frac{\bar{E}}{\bar{y}_e}\rvert_{\max}$ %	$\lvert\frac{CI}{\bar{y}_e}\rvert_{\max}$ %
k–ε	Zeman	12.3	8.3	32.9	9.9
k–ω	Zeman	14.6	8.3	43.8	16.4
k–ε	Sarkar	18.1	8.3	38.9	9.7
k–ω	Sarkar	13.3	8.3	34.9	16.4
k–ε	Wilcox	23.1	8.3	52.5	9.9
k–ω	Wilcox	11.9	8.3	30.1	10.5

with respect to the width of the confidence interval at the x value where $|\bar{E}/\bar{y}_e|$ achieves its maximum, denoted $|CI/\bar{y}_e|_{\max}$.

Table 5 gives the average relative error and maximum relative error over the range $0 \leq M_c \leq 1.5$ for all models considered. These results should be interpreted together with the average width of the confidence interval, which was 8.3% at 90% confidence, and the confidence interval width at maximum relative error, listed in the table. Thus, for the k–ε/Zeman model, one would state that the average relative error is $12.3 \pm 8.3\%$ at 90% confidence, and the maximum relative error is $32.9 \pm 9.9\%$ at 90% confidence. Note that for all the models, the maximum error is much larger than the average error. Referring to Fig. 8, this is due to one of two reasons: the inability of the model to predict the steep drop in turbulent mixing between $M_c = 0.5$ and $M_c = 1.0$, as with the k–ε results, or the inability of the model to predict the leveling off of the compressibility factor for $M_c > 1.0$, as with the k–ω results. The average error of about 12% for the best two (existing) models, though not alarmingly large, is slightly larger than the average experimental confidence interval of 8.3%.

We emphasize that judgements regarding the adequacy of these models for a particular task must always be made while taking into consideration the accuracy requirements of the application at hand. The validation metric is a passive measure of model performance; by itself, it does not determine if a model is "good enough." A further observation is that if a model were required to have a relative error of less than 8.3% on average at 90% confidence over this range of convective Mach number, more experimental data points would be needed to attain the required accuracy assessment.

Conclusions

A recommended data set for compressible shear layer growth rate has been constructed and used to assess several compressibility corrections to two-equation turbulence models for mixing layer flows. A validation metric formulation was used to compare the computational prediction with experimental data. The validation metric allowed for weaknesses in the models over certain input parameter ranges to be highlighted relative to the confidence in the available experimental data over the same input parameter range. Global metrics allowed for concise quantitative statements to be made regarding the accuracy of each model considered.

While all the models predict a decrease in growth rate with increasing convective Mach number, the average relative error in compressibility factor is larger than 10% over the convective Mach number range $0 \leq M_c \leq 1.5$, with much larger maxima in relative error occurring over this range. The k–ε model with the Zeman compressibility correction and the Wilcox k–ω model with the Wilcox compressibility correction gave the lowest average relative error over the convective Mach number range considered. The average relative error for both models was about 12%, whereas the highest average relative error of 23% was obtained for the k–ε model with the Wilcox compressibility correction. These results, along with the more vexing fact that the compressibility corrections (as is now known) are grounded in incorrect physical assumptions, point to the need for better models for compressible turbulence. While the validation metric results reveal deficiencies in models, they do not give detailed insight into the validity of particular modeling assumptions. Further theoretical and direct simulation work is required to gain further insight.

Finally, note that validation studies point out weaknesses in experimental data sets as well as in computational models. The confidence intervals computed for the present experimental data set are widest at larger convective Mach numbers. This indicates that new data are needed to firmly establish the correct trend for mixing layer growth-rate reduction for convective Mach numbers greater than 1.0.

Acknowledgements

The authors are grateful for the technical reviews of this work provided by Ryan Bond and Tim O'Hern of Sandia National Laboratories. Sandia is a multiprogram laboratory operated by Sandia Corporation, a Lockheed Martin Company for the United States Department of Energy's National Nuclear Security Administration under Contract DE-AC04-94AL85000.

References

[1] Oberkampf, W. L., and Barone, M. F., "Measures of Agreement Between Computation and Experiment: Validation Metrics," AIAA Paper 2004-2626, June 2004.

[2] Oberkampf, W. L., and Barone, M. F., "Measures of Agreement Between Computation and Experiment: Validation Metrics," *Journal of Computational Physics* (to be published).

[3] Bogdanoff, D. W., "Compressibility Effects in Turbulent Shear Layers," *AIAA Journal*, Vol. 21, No. 6, 1983, pp. 926–927.

[4] Lele, S. K., "Compressibility Effects on Turbulence," *Annual Review of Fluid Mechanics*, Vol. 26, Jan. 1994, pp. 211–254.

[5] Smits, A. J., and Dussauge, J., *Turbulent Shear Layers in Supersonic Flow*, AIP Press, New York, 1996, Chap. 6.

[6] Birch, F., and Eggers, J. M., "A Critical Review of the Experimental Data for Developed Free Turbulent Shear Layers," *Free Turbulent Shear Flows, Volume I: Conference Proceedings*, SP-321, NASA, NASA Scientific and Technical Office, 1973.

[7] Barre, S., Quine, C., and Dussauge, J. P., "Compressibility Effects on the Structure of Supersonic Mixing Layers: Experimental Results," *Journal of Fluid Mechanics*, Vol. 259, Jan. 1994, pp. 47–78.

[8] Barre, S., Braud, P., Chambres, O., and Bonnet, J. P., "Influence of Inlet Pressure Conditions on Supersonic Turbulent Mixing Layers," *Experimental Thermal and Fluid Science*, Vol. 14, No. 1, 1997, pp. 68–74.

[9] Dutton, J. C., "Compressible Turbulent Free Shear Layers," AGARD, Rept. 819, 1997.

[10] Barre, S., Bonnet, J.-P., Gatski, T. B., and Sandham, N. D., "Compressible, High Speed Flows, *Closure Strategies for Turbulent and Transitional Flows*, edited by B. Launder and N. Sandham, Cambridge Univ. Press, Cambridge, England, U.K., 2002, Chap. 19.

[11] Papamoschou, D., and Roshko, A., "The Compressible Turbulent Shear Layer: An Experimental Study," *Journal of Fluid Mechanics*, Vol. 197, Dec. 1988, pp. 453–477.

[12] Schlichting, H., *Boundary-Layer Theory*, 7th ed., McGraw–Hill, New York, 1979.

[13] Brown, G. L., "The Entrainment and Large Structure in Turbulent Mixing Layers," *Proceedings of the 5th Australasian Conference on Hydraulics and Fluid Mechanics*, Canterbury Univ., Christchurch, New Zealand, 1974.

[14] Schetz, J. A., *Boundary Layer Analysis*, Prentice Hall, Englewood Cliffs, NJ, 1993.

[15] Samimy, M., and Elliott, G. S., "Effects of Compressibility on the Characteristics of Free Shear Layers," *AIAA Journal*, Vol. 28, No. 3, March 1990, pp. 439–445.

[16] Elliott, G. S., and Samimy, M., "Compressibility Effects in Free Shear Layers," *Physics of Fluids A*, Vol. 2, No. 7, July 1990, pp. 1231–1240.

[17] Chinzei, N., Masuya, G., Komuro, T., Murakami, A., and Kudou, K., "Spreading of Two-Stream Supersonic Turbulent Mixing Layers," *Physics of Fluids*, Vol. 29, May 1986, pp. 1345–1347.

[18] Goebel, S. G., and Dutton, J. C., "Experimental Study of Compressible Turbulent Mixing Layers," *AIAA Journal*, Vol. 29, April 1991, pp. 538–546.

[19] Dutton, J. C., Burr, R. F., Goebel, S. G., and Messersmith, N. L., "Compressibility and Mixing in Turbulent Free Shear Layers," *12th Symposium on Turbulence*, University of Missouri–Rolla, Rolla, MO, Sept. 1990.

[20] Gruber, M. R., Messersmith, N. L., and Dutton, J. C., "Three-Dimensional Velocity Field in a Compressible Mixing Layer," *AIAA Journal*, Vol. 31, Nov. 1993, pp. 2061–2067.

[21] Debisschop, J. R., and Bonnet, J. P., "Mean and Fluctuating Velocity Measurements in Supersonic Mixing Layers," *Engineering Turbulence Modeling and Experiments 2*, edited by W. Rodi and F. Martelli, Elsevier, New York, 1993.

[22] Debisschop, J. R., Chambres, O., and Bonnet, J. P., "Velocity-Field Characteristics in Supersonic Mixing Layers," *Experimental Thermal and Fluid Science*, Vol. 9, Aug. 1994, pp. 147–155.

[23] Barre, S., Braud, P., Chambres, O., and Bonnet, J. P., "Influence of Inlet Pressure Conditions on Supersonic Turbulent Mixing Layers," *Experimental Thermal and Fluid Science*, Vol. 14, No. 1, 1997, pp. 68–74.

[24] Pantano, C., and Sarkar, S., "A Study of Compressibility Effects in the High-Speed Turbulent Shear Layer Using Direct Simulation," *Journal of Fluid Mechanics*, Vol. 451, Jan. 2002, pp. 329–371.

[25] Zeman, O., "Dilatation Dissipation: The Concept and Application in Modeling Compressible Mixing Layers," *Physics of Fluids A*, Vol. 2, No. 2, Feb. 1990, pp. 178–188.

[26] Sarkar, S., Erlebacher, G., Hussaini, M. Y., and Kreiss, H. O., "The Analysis and Modeling of Dilatational Terms in Compressible Turbulence," ICASE, Rept. 89-79, 1989.

[27] Wilcox, D. C., "Dilatation-Dissipation Corrections for Advanced Turbulence Models, *AIAA Journal*, Vol. 30, No. 11, Nov. 1992, pp. 2639–2646.

[28] Vreman, A. W., Sandham, N. D., and Luo, K. H., "Compressible Mixing Layer Growth Rate and Turbulence Characteristics" *Journal of Fluid Mechanics*, Vol. 320, Aug. 1996, pp. 235–258.

[29] Freund, J. B., Moin, P., and Lele, S. K., "Compressibility Effects in a Turbulent Annular Mixing Layer. Part 1, Turbulence and Growth Rate," *Journal of Fluid Mechanics*, Vol. 421, Oct. 2000, pp. 229–267.

[30] Wilcox, D. C., *Turbulence Modeling for CFD*, 2nd ed., third printing, DCW Industries, La Cañada, CA, 2002.

[31] Viegas, J. R., and Rubesin, M. W., "Assessment of Compressibility Corrections to the $k-\varepsilon$ Model in High-Speed Shear Layers," *AIAA Journal*, Vol. 30, No. 10, Oct. 1992, pp. 2369–2370.

[32] Adumitroaie, V., Ristorcelli, J. R., and Taulbee, D. B., "Progress in Favré–Reynolds Stress Closures for Compressible Flows," *Physics of Fluids*, Vol. 11, No. 9, 1999, pp. 2696–2719.

[33] Aupoix, B., "Modelling of Compressibility Effects in Mixing Layers," *Journal of Turbulence*, Vol. 5, Feb. 2004, pp. 1–17.

[34] Launder, B. E., and Sharma, B. I., "Application of the Energy Dissipation Model of Turbulence to the Calculation of Flow near a Spinning Disc," *Letters in Heat and Mass Transfer*, Vol. 1, No. 2, 1974, pp. 131–138.

[35] Nagano, Y., and Hishida, M., "Improved Form of the $k-\varepsilon$ Model for Wall Turbulent Shear Flows, *Journal of Fluids Engineering*, Vol. 109, June 1987, pp. 156–160.

[36] Wong, C. C., Blottner, F. G., Payne, J. L., and Soetrisno, M., "Implementation of a Parallel Algorithm for Thermochemical Nonequilibrium Flow Solutions," AIAA Paper 95-0152, Jan. 1995.

[37] Wong, C. C., Soetrisno, M., Blottner, F. G., Imlay, S. T., and Payne, J. L., "PINCA: A Scalable Parallel Program for Compressible Gas Dynamics with Nonequilibrium Chemistry," Sandia National Labs, Rept. SAND 94-2436, Albuquerque, NM, April 1995.

[38] Yee, H. C. "Implicit and Symmetric Shock Capturing Schemes," NASA, TM-89464, May 1987.

[39] Yoon, S., and Jameson, A., "An LU-SSOR Scheme for the Euler and Navier–Stokes Equations," AIAA Paper 87-0600, 1987.

[40] Bradshaw, P., "Compressibility Effects on Free-Shear Layers," *Conference on Complex Turbulent Flows*, edited by S. J. Kline, B. J. Cantwell, and G. M. Lilley, Vol. 1, Stanford Univ., Stanford, CA, 1981, pp. 364–368.

[41] Rubel, A., and Melnik, R. E., "Jet, Wake, and Wall Jet Solutions Using a $k-\varepsilon$ Turbulence Model," AIAA Paper 84-1523, 1984.

[42] Roache, P. J., *Verification and Validation in Computational Science and Engineering*, Hermosa Publishers, Albuquerque, NM, 1998.

[43] Roy, C. J., McWherter-Payne, M. A., and Oberkampf, W. L, "Verification and Validation for Laminar Hypersonic Flowfields, Part I: Verification, *AIAA Journal*, Vol. 41, No. 10, 2003, pp. 1934–1943.

[44] Paciorri, R., and Sabetta, F., "Compressibility Correction for the Spalart-Allmaras Model in Free-Shear Flows, *Journal of Spacecraft and Rockets*, Vol. 40, No. 3, May–June 2003, pp. 326–331.

P. Givi
Associate Editor